Phototransistors development and their applications to Lidar

M.N. Abedin[1], T.F. Refaat[2], S. Ismail[1], and U.N. Singh[1]

[1]NASA Langley Research Center, Hampton, VA 23681
[2]Old Dominion University, Norfolk, VA 23529

Abstract **- Custom-designed two-micron phototransistors have been developed using Liquid Phase Epitaxy (LPE), Molecular Beam Epitaxy (MBE) and Metal-Organic Chemical Vapor Deposition (MOCVD) techniques under Laser Risk Reduction Program (LRRP). The devices were characterized in the Detector Characterization Laboratory at NASA Langley Research Center. It appears that the performance of LPE- and MBE-grown phototransistors such as responsivity, noise-equivalent-power, and gain, are better than MOCVD-grown devices. Lidar tests have been conducted using LPE and MBE devices under the 2-µm CO_2 Differential Absorption Lidar (DIAL) Instrument Incubator Program (IIP) at the National Center for Atmospheric Research (NCAR), Boulder, Colorado. The main focus of these tests was to examine the phototransistors' performances as compared to commercial InGaAs avalanche photodiode by integrating them into the Raman-shifted Eye-safe Aerosol Lidar (REAL) operating at 1.543 µm. A simultaneous measurement of the atmospheric backscatter signals using the LPE phototransistors and the commercial APD demonstrated good agreement between these two devices. On the other hand, simultaneous detection of lidar backscatter signals using MBE-grown phototransistor and InGaAs APD, showed a general agreement between these two devices with a lower performance than LPE devices. These custom-built phototransistors were optimized for detection around 2-µm wavelength while the lidar tests were performed at 1.543 µm. Phototransistor operation at 2-micron will improve the performance of a lidar system operating at that wavelength. Measurements include detecting hard targets (Rocky Mountains), atmospheric structure consisting of cirrus clouds and boundary layer. These phototransistors may have potential for high sensitivity differential absorption lidar measurements of carbon dioxide and water vapor at 2.05-µm and 1.9-µm, respectively.**

I. INTRODUCTION

NASA's Earth Science Technology Office provided fund to develop 2-micron detectors within the Laser Risk Reduction Program (LRRP), which have numerous applications for atmospheric monitoring, such as profiling CO_2, H_2O, CO, and CH_4. NASA Langley detector group, in partnership with AstroPower and later with University of Delaware, took the initiative to develop novel phototransistors using three methods, which are Liquid Phase Epitaxy (LPE), Molecular Beam Epitaxy (MBE), and Metal Organic Chemical Vapor Deposition (MOCVD). In order to satisfy the requirements of the active remote sensing applications, detector selection must be based on the performance parameters, such as high spectral response, high quantum efficiency, low noise-equivalent-power (NEP), and high gain. In general, a large area detector operating in the 1.0- to 2.5-µm

wavelength range is the detectors of choice for the next generation Earth and Space Science remote sensing, Mars Orbiter and planetary instruments. Besides p-i-n photodiodes and APDs, antimonide (Sb)-based heterojunction phototransistors (HPT) attracted a great attention to satisfy many of the detector requirements for applications to the active and passive remote sensing systems without the excess noise problem and with lower operating bias voltages [1-4]. HPT has an internal gain mechanism that allows increasing the output signal and signal-to-noise ratio (SNR).

Quaternary AlGaAsSb/InGaAsSb heterojunction phototransistors operating in the 1.0 to 2.2 μm wavelength range have been developed and fabricated at AstroPower, Inc. in collaboration with NASA Langley Research Center using LPE method [3, 5-8]. In addition, MBE and MOCVD growth methods were employed to fabricate HPTs at the University of Delaware. The last two methods provide better control over doping levels, composition and width of the AlGaAsSb and InGaAsSb layers with respect to LPE method. These devices have been characterized at NASA Langley Research Center, and encouraging results including high responsivity, high detectivity, and relatively low NEP have been obtained. It appears that the LPE-grown phototransistor's performances, such as responsivity, NEP, and gain, are better than MBE- and MOCVD-grown phototransistors.

To validate the phototransistors' performances, lidar tests have been carried out at National Center for Atmospheric Research (NCAR), Boulder, Colorado. HPTs were integrated into the REAL system operating at 1.543 micron [9-10]. This study was supported by 2-μm CO_2 Differential Absorption Lidar (DIAL) Instrument Incubator Program (IIP). The main focus of these tests was to acquire lidar backscatter signals through the phototransistor (LPE or MBE) and InGaAs APD (Perkin Elmer, Model#C30659-1550-R2A) channels simultaneously for comparing the phototransistor performance with respect to the InGaAs APD. These custom-built phototransistors were optimized for detection around 2-μm wavelength and the lidar tests were performed at 1.543 μm. Therefore, the REAL system serves as a useful test-bed for validation of the phototransistor by measuring the returns from hard targets (Rocky Mountains), atmospheric structure consisting of clouds and boundary layer [10]. Finally, Sb-based phototransistors have been tested to validate their performances at 1.543-μm and would enhance the capability for active remote sensing of CO_2 and water vapor at 2.05 and 1.9 μm, respectively.

II. PHOTOTRANSISTOR FABRICATION

A major study of this effort is to determine the best geometrical parameters for the material system to achieve efficient photo-detection in the wavelength of interest with reduced dark current. $Ga_xIn_{1-x}As_ySb_{1-y}$ material combination lattice-matched to GaSb substrate was considered as a point of reference. Single element detectors were grown on the substrate and optimized with vertically integrated 4-layers n-p-p-n structures. Figure 1 shows the general fabricated HPT mesa structure for LPE-, MBE-, and MOCVD-grown phototransistors [5, 11-12]. Three different compositions of quaternary alloys were used to provide the cutoff wavelength (50% QE of peak wavelength) of 2.1 μm (LPE), 2.4 μm (MBE) and 2.15 μm (MOCVD). The MBE HPT was composed of $Al_{0.25}Ga_{0.75}As_{0.02}Sb_{0.98}$ and $In_{0.18}Ga_{0.82}As_{0.17}Sb_{0.83}$ layers with room-temperature bandgaps of $Eg \approx 1.0$ eV and $Eg \approx 0.54$ eV, respectively [11-12]. The layers are lattice-matched to a GaSb substrate. The growth started with a 0.15-μm thick n^+-GaSb

buffer layer and was completed with a 0.1-μm thick n^+- GaSb contact layer doped with Te. The HPT structure includes a 0.5-μm thick n-type AlGaAsSb emitter, 0.8-μm thick p-type composite base consisting of AlGaAsSb (0.3-μm) and InGaAsSb (0.5 μm) layers, and a 1.5-μm thick n-type InGaAsSb collector. The MOCVD HPT differs by a higher bandgap $In_{0.16}Ga_{0.84}As_{0.14}Sb_{0.86}$ layers with a room-temperature bandgap of $Eg \approx 0.555$ eV [12].

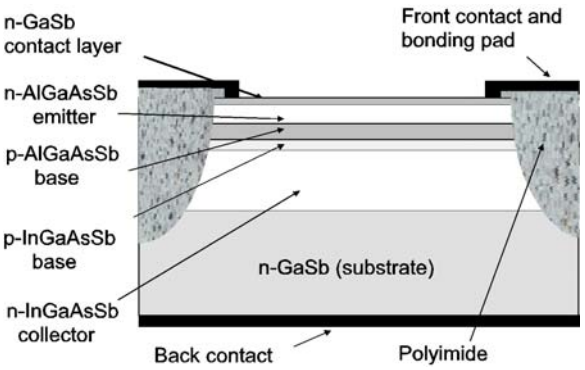

Figure 1. General phototransistor structure of the fabricated AlGaAsSb/InGaAsSb material system.

The details of the LPE, MBE, and MOCVD techniques used for the growth of the device structures were discussed in more detailed elsewhere [5,11-12]. The fabrication process of the mesa HPTs involved photolithography and wet chemical etching. Backside planar and front side annular ohmic contacts (together with a bonding pad) were deposited by electron-beam evaporation of Au/Ge. A polyimide coating (HD Microsystems PI-2723 photodefinable polyimide resin) was spun on the front of the device. The polyimide served several functions including planarization of the top surface, mesa isolation, and edge passivation. After dicing 1-mm² pieces, with a single device in the middle of each square, the devices were mounted on to TO-18 headers using silver conducting epoxy and wire-bonded. No antireflection coatings were applied.

III. PHOTOTRANSISTOR CHARACTERIZATION

NASA LaRC detector group carried out comprehensive device characterization, including spectral response, dark current, and noise measurements. Analysis of the detector characterization included quantum efficiency, detectivity (D*), and NEP calculations. The phototransistor was integrated into an ILX Lightwave chamber with cooling system. Focusing on phototransistors with 200-, 300-, and 1000-μm diameter (LPE, MBE, and MOCVD), figure 2 shows the responsivity variation with wavelength in the 1.0- to 2.7-μm range. The results show complicated composition dependence cutoff wavelengths at 2.1-, 2.4-, and 2.15-μm with operating temperature at 20°C and 0.0 V bias. The peak responsivities around 1.4 A/W for LPE, 0.75 A/W for MBE, and 0.25 A/W for MOCVD were detected at 2.0-, 2.08-, and 2.2-μm wavelengths. The highest responsivity was detected from the LPE phototransistor (red solid line) as compared to MBE (green) and MOCVD (blue) devices at these operating conditions.

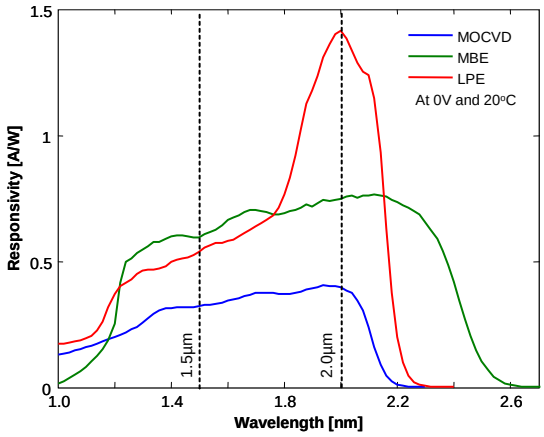

Figure 2. Spectral Response calibration of LPE, MBE, and MOCVD phototransistors at 0 V and 20°C.

Fig. 3 shows the NEP of the phototransistors as a function of wavelength, obtained at the optimum bias voltages and 20°C. The bias dependencies of NEP can be considered for an optimum operation of the phototransistors. Comparing these three phototransistors, the NEP (red solid line) is determined around two orders-of-magnitude lower for LPE (20 °C) as compared to MOCVD (blue solid line) (20 °C) at 2.05-μm radiation with 3.5 V and 0.8 V bias, respectively and similar with respect to MBE (green solid line) at 2.05-μm radiation with 1.4 V and 0.8 V, respectively. For the measured NEP for the phototransistor device at 2.05-μm radiation wavelength region, the bias dependence of NEP (bottom red solid line: NEP ~ 8.0×10^{-13} W/Hz$^{1/2}$ at 20 °C) is around 100 times smaller at 3.5 V with respect to MOCVD phototransistor (NEP ~ 3.0×10^{-9} W/Hz$^{1/2}$ at 20 °C). Comparison with the best of the tested Sb-based phototransistor measured at 20 °C shows that at 3.5 V the phototransistor achieves near two orders of magnitude lower NEP despite the four times smaller diameter. Besides 300-μm phototransistor diameter, MBE phototransistor was also operated at 20 °C and NEP was measured as low as 1.0×10^{-12} W/Hz$^{1/2}$ with incident radiation of 2.05 μm at 1.4 V. The bias dependence of NEP for the MOCVD phototransistor showed a small increase of the noise, but it has a limited gain by applying high bias voltage (saturation voltage of 0.8 V). Therefore the overall NEP was higher than that of LPE and MBE devices.

The HPT's gain was calculated as a function of incident radiation at 20 °C and optimum bias voltage for each type of phototransistor. This gain was determined by measuring the responsivity (R_T) of the HPT as a function of bias voltage at a specific wavelength and temperature. This gain (g) can be determined using the following equation [13]:

$$g = R_T(\lambda,V,T) / R_T(\lambda,0,T) \quad (1)$$

where $R_T(\lambda,V,T)$ is the responsivity, which depends on incident photon wavelength (λ), applied bias voltage (V), and temperature (T).

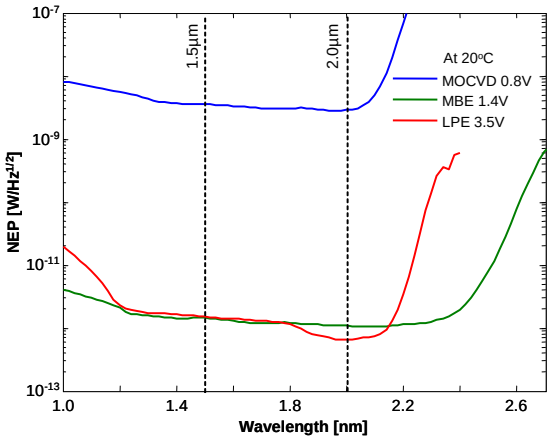

Figure 3. NEP determination of LPE, MBE, and MOCVD phototransistors with optimum bias voltage at 20 °C.

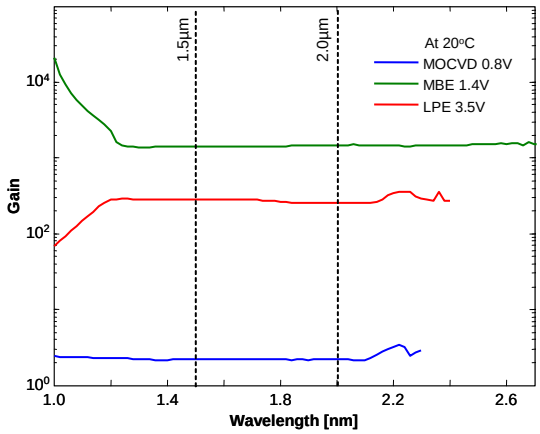

Figure 4. Gain variation as a function of wavelength for LPE, MBE, and MOCVD phototransistors with optimum bias voltage and 20 °C.

Figure 4 shows the gain versus wavelength (λ) for HPT calculated using equation 1. A gain of about 200 is obtained at 3.5 V, ~1800 is obtained at 1.4 V, and ~3 is obtained at 0.8 V optimum voltages for LPE

(red), MBE (green), and MOCVD (blue) approaches, respectively. It is observed that the gain of HPTs is bias dependence.

IV. PHOTOTRANSISTOR VALIDATION AT NCAR

Based on characterization and performance analysis, the LPE- and MBE-grown phototransistors were selected to be validated by integrating them into a lidar receiver system, which is the part of the NCAR's REAL system. The atmospheric backscatter signals were collected and then compared with the InGaAs APD of the REAL system. REAL comprises of transmitter and receiver subsystems and the characteristics of which are discussed in the following.

The transmitter subsystem consists of the 1.064 μm Nd:YAG pulsed laser, which is passed through a Raman cell (CH_4) and converts 1.543 μm Raman-shifted Stokes line. This 1.543 μm Raman-shifted line transmits to the target with energy 220 mJ, repetition rate 10 Hz, beam divergence (half-angle) 0.20x0.24 mrad, beam quality M^2 = 3x3 of Nd:YAG pump and M^2 = 10x12 of Stokes beam, transmitted beam diameter 50 mm, and pulse width 4 ns (FWHM). The backscatter signals are collected by the receiver subsystem, which consists of the 40 cm (diameter) telescope with field-of-view 0.27 mrad (half-angle), filter bandwidth 5 nm, 200-μm APD (InGaAs), digitizer sampling rate of 50 MHz, and resolution of 14-bit. The polarization beam splitter cube is used to split backscatter signal into two equivalently energetic beams and focused them onto two independent detectors (one is for APD and other one is phototransistor). The detailed discussion of the transmitter and receiver components, and the integrated REAL setup was reported in Refs. 9 - 10.

V. ATMOSPHERIC RETURN AND DISCUSSION

Selected phototransistors were employed to record the atmospheric returns and compared their features with commercial APD. The phototransistor attached with thermo-electric cooler (TEC) and trans-impedance amplifier was integrated into REAL system at NCAR, Boulder, Colorado on June 8, 2006. TEC was used to operate the phototransistor at fixed temperature (20 ^{o}C). Lidar system was aligned using a 14 km mountaintop as hard target with elevation angle 3.4^{o}, as specified in signal profiles for both channels in Figures 5a and 5b. The atmospheric returns in Figure 5 are represented by the digitizer output in counts in the vertical axis and the digitizer output in range (km) in the horizontal axis.

The return signals from hard target were detected simultaneously by the phototransistor and the APD. Figure 5a (Top - white trace: LPE phototransistor and pink trace: APD) showed hard target signals at 14 km distance through LPE-grown phototransistor and InGaAs APD and near comparable signals were obtained. Figure 5b (Bottom - white trace: MBE phototransistor and pink trace: APD) showed hard target signals from two mountains' tops at 9.8 km and 14-km distances using MBE-grown phototransistor and InGaAs APD. It was observed that small amplitude signals from the two targets were detected by the MBE-grown phototransistor, but large signals from the same hard targets were monitored by the APD.

The MBE-grown phototransistor suffers higher noise and longer recovery time, which could affect the overall performance of the return signals. On the other hand, LPE-grown phototransistor has lower noise and shorter recovery time as compared to MBE-grown phototransistor. Therefore, the comparable signal of the LPE-grown phototransistor with respect to the InGaAs APD is shown in Figure 5a.

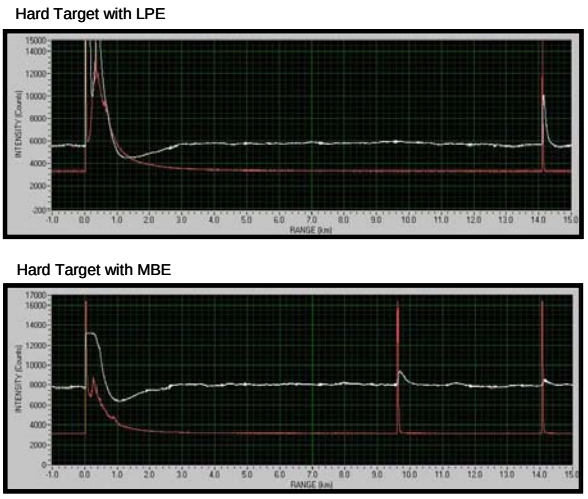

Figure 5. Atmospheric return signals using LPE, MBE, and InGaAs APD.

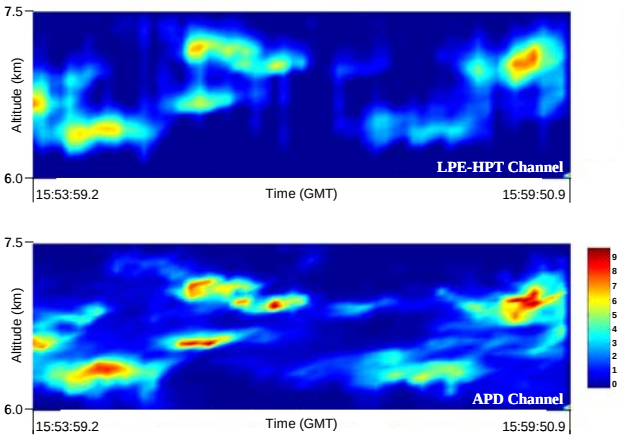

Figure 6. Atmospheric images using LPE and APD (60 shot average and 10 running average)

The REAL system was also pointed vertically to collect atmospheric returns through both channels. Figure 6 shows atmospheric features of the return signals for the LPE-grown phototransistor (Top image) and APD (Bottom image) channels. The system was pointed at thin discrete clouds at about 6.5-7.0 km altitudes. The color image represents the backscattered range corrected signal. The time scale represents the time span between 15:54 to 15:60 GMT, which corresponds to the phototransistor and APD operating time at a temperature of 20 ^{o}C. Near to similar results obtained between the LPE-grown phototransistor and APD channels and this indicates potential application of the phototransistor for lidar remote sensing. There is also some discrepancy observed between these two channels that could be due to an electronic overshoot problem of the phototransistor driving circuitry.

Figure 7 shows similar atmospheric features of the return signals for the MBE-grown phototransistor and APD channels. The color image presented in Figures 7a (Top image- MBE phototransistor) and 7b (Bottom image- APD) were analyzed with 60 shot averages, equivalent to 6 s, and 10 running average. The corrected range spans between 7.4 to 9.4 km altitudes. The time scale spans between 15:54 to 15:60 GMT, which corresponds to the phototransistor and APD operating time at a temperature of 20 ^{o}C.

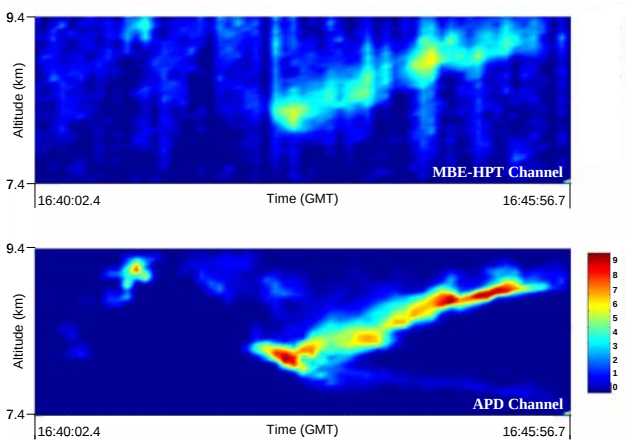

Figure 7. Atmospheric return images using MBE and APD (60 shot average and 10 running average).

Results show some discrepancy as indicated in Figures 7a and 7b, which might be due to the existing overshoot problem of the phototransistor's associated electronics including relatively high noise and long recovery time of MBE-grown phototransistor. It is interestingly enough to discuss that these

phototransistors were developed and optimized for 2-μm wavelength operation, but LPE-grown phototransistor has a comparable performance with respect to InGaAs APD at 1.5-μm wavelength. Phototransistor operation at 2-μm will further enhance the performance (for example, higher responsivity and higher QE) and enhance the SNR by reducing the dark current and device noise at lower operating temperature (-20 ^{o}C) [10].

VI. SUMMARY

In summary, quaternary AlGaAsSb/InGaAsSb heterojunction phototransistors were developed at AstroPower, Inc. and the University of Delaware in collaboration with NASA Langley Research Center using LPE, MBE and MOCVD methods. These HPTs were characterized at NASA Langley Research Center and results obtained including high responsivity, high detectivity, and relatively low NEP. It was worth mentioning that both LPE and MBE-grown phototransistor's performances, such as responsivity, noise-equivalent-power, and gain, were better than MOCVD-grown phototransistors.

These custom-built phototransistors were developed and optimized for 2-μm wavelength operation. These phototransistors were validated at 1.5-μm wavelength by integrating them into the REAL system at NCAR, Boulder, Colorado. LPE devices show comparable performance with respect to InGaAs APD operating at 1.5-μm. Operation at 2-μm will further enhances the performance of lidar system by increasing the responsivity and doubles the quantum efficiency leading to enhance the SNR. Results indicated an acceptable performance of the phototransistor devices, in terms of detecting hard targets and atmospheric structures including discrete clouds at 6.5-7.0 km and 7.4 to 9.4 km altitudes.

AKNOWLEDGEMENT

This work is supported by Laser Risk Reduction Program and 2-μm CO_2 DIAL IIP Project under NASA's Earth Science Technology Office and NASA's Enabling Concepts & Technologies Program. The authors would like to thanks Oleg Sulima from University of Delaware for fabricating the phototransistors and Terry Mack for phototransistor electronics; Scott Spuler and Shane Mayor from NCAR to provide lab and also assist to operate the REAL System. The authors also acknowledge George Komar and William Stabnow for their constant support.

REFERENCES

[1] P. Ambrico, A. Amodeo, P. Girolamo, and N. Spinelli, Sensitivity analysis of differential absorption lidar measurements in the mid-infrared region, Applied Optics 39(36), 6847– 6865 (2000).

[2] S. Ismail, G. J. Koch, B. W. Barnes, N. Abedin, T. F. Refaat, J. Yu, S. A. Vay, S. A. Kooi, E. V. Browell, U. N. Singh, Technology Developments for Tropospheric Profiling of CO_2 and Ground-based Measurements, Proceedings of the 22nd International Laser Radar Conference, 65-68 (2004).

[3] T.F. Refaat, M.N. Abedin, O.V. Sulima, S. Ismail, and U.N. Singh, AlGaAsSb/InGaAsSb phototransistors for 2-μm remote sensing applications, Optical Engineering 43(7), 1647-1650 (2004).

[4] T.F. Refaat, M.N. Abedin, O.V. Sulima, U.N. Singh, and S. Ismail, Novel infrared phototransistors for atmospheric CO_2 profiling at 2 μm wavelength, IEDM Tech. Dig., 355-358 (2004).

[5] O.V. Sulima, T.F. Refaat, M.G. Mauk, J.A. Cox, J. Li, S.K. Lohokare, M.N. Abedin, U.N. Singh, and J.A. Rand, AlGaAsSb/InGaAsSb phototransistors for spectral range around 2-μm, Electronics

Letters 40, 766-767, (2004).
[6] O.V. Sulima, T.F. Refaat, M.G. Mauk, J.A. Cox, J. Li, S.K. Lohokare, M.N. Abedin, U.N. Singh, and J.A. Rand, Novel AlGaAsSb/InGaAsSb phototransistors for spectral range 2.0 - 2.1 μm, presented at 6th Middle-Infrared Optoelectronics Materials and Devices (MIOMD) Conference, in St. Petersburg, Russia, 28 June-1 July 2004.
[7] M.N. Abedin, T.F. Refaat, O.V. Sulima, and U.N. Singh, "AlGaAsSb/InGaAsSb heterojunction phototransistors with high optical gain and wide dynamic range", IEEE Trans. Electron Devices 51(12), 2013-2018 (2004).
[8] M.N. Abedin, T.F. Refaat, O.V. Sulima, and U.N. Singh, "Recent development of Sb-based phototransistors in the 0.9- to 2.2-μm wavelength range for applications to laser remote sensing", Int. J. High Speed Electronics and Systems, 16 (2), 567-582 (2006).
[9] S. Mayor and S. Spuler, "Raman-shifted eye-safe aerosol lidar", Applied Optics, 43(19), 3915-3924 (2004).
[10] T.F. Refaat, S. Ismail, T. Mack, M.N. Abedin, S. Mayor, S. Spuler, and U.N. Singh, "Infrared Phototransistor Validation for Atmospheric Remote Sensing Application using the Raman-Shifted Eye-Safe Aerosol Lidar (REAL), Optical Engineering, 46(8), (2007)", accepted.
[11] O.V. Sulima, K. Swaminathan, T.F. Refaat, N.N. Faleev, A.N. Semenov, V.A. Solov'ev, S.V. Ivanov, M.N. Abedin, U.N. Singh, and D. Prather, "2.4 micron cutoff wavelength AlGaAsSb/InGaAsSb phototransistors", Electronics Letters, 42 (1), 55-56 (2006).
[12] K. Swaminathan, O.V. Sulima, T.F. Refaat, T. Dillon, E. Marchena, N.N. Faleev, M.N. Abedin, U.N. Singh, and D. Prather, "Room temperature AlGaAsSb/InGaAsSb heterojunction phototransistors", Proc SPIE 6232, 62320P (2006).
[13] M.N. Abedin, T.F. Refaat, O.V. Sulima, S. Ismail, and U.N. Singh, "Two-micron detector development using Sb-based material systems", 6th Annual Earth Science Technology Conference, NASA's Earth Science Technology Office, b1p3, (2006).